ResearchGate

See discussions, stats, and author profiles for this publication at: https://www.researchgate.net/publication/263941907

# Enhanced Li Adsorption and Diffusion on MoS2 Zigzag Nanoribbons by Edge Effects: A Computational Study

**ARTICLE** *in* JOURNAL OF PHYSICAL CHEMISTRY LETTERS · AUGUST 2012

Impact Factor: 7.46 · DOI: 10.1021/jz300792n

CITATIONS
55

READS
204

**5 AUTHORS**, INCLUDING:

Zhen Zhou
Nankai University
**213** PUBLICATIONS **6,983** CITATIONS
SEE PROFILE

Carlos R Cabrera
University of Puerto Rico at Rio Piedras
**197** PUBLICATIONS **2,658** CITATIONS
SEE PROFILE

Zhongfang Chen
University of Puerto Rico at Rio Piedras
**221** PUBLICATIONS **8,040** CITATIONS
SEE PROFILE

Available from: Zhen Zhou
Retrieved on: 29 January 2016

THE JOURNAL OF PHYSICAL CHEMISTRY Letters

Letter

pubs.acs.org/JPCL

# Enhanced Li Adsorption and Diffusion on $MoS_2$ Zigzag Nanoribbons by Edge Effects: A Computational Study

Yafei Li,[†,‡] Dihua Wu,[†] Zhen Zhou,[†,*] Carlos R. Cabrera,[‡] and Zhongfang Chen[‡,*]

[†]Tianjin Key Laboratory of Metal and Molecule Based Material Chemistry, Key Laboratory of Advanced Energy Materials Chemistry (Ministry of Education), Computational Centre for Molecular Science, Institute of New Energy Material Chemistry, Nankai University, Tianjin 300071, China

[‡]Department of Chemistry, Institute for Functional Nanomaterials, University of Puerto Rico, Rio Piedras Campus, San Juan, PR 00931

Supporting Information

**ABSTRACT:** By means of density functional theory computations, we systematically investigated the adsorption and diffusion of Li on the 2-D $MoS_2$ nanosheets and 1-D zigzag $MoS_2$ nanoribbons ($ZMoS_2NRs$), in comparison with $MoS_2$ bulk. Although the Li mobility can be significantly facilitated in $MoS_2$ nanosheets, their decreased Li binding energies make them less attractive for cathode applications. Because of the presence of unique edge states, $ZMoS_2NRs$ have a remarkably enhanced binding interaction with Li without sacrificing the Li mobility, and thus are promising as cathode materials of Li-ion batteries with a high power density and fast charge/discharge rates.

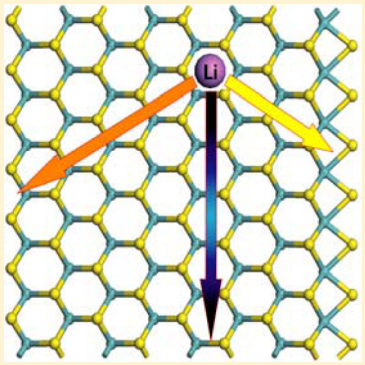


**SECTION:** Energy Conversion and Storage; Energy and Charge Transport

Molybdenum disulfide ($MoS_2$), a typical layered inorganic material, structurally well resembles graphite. However, instead of a layered planar structure in graphite, $MoS_2$ is constructed by triple atomic layers, in which Mo atoms in the trigonal prismatic coordination are sandwiched between two layers of pyramidal S atoms. Similar to graphite, these $MoS_2$ layers are held together by the weak van der Waals (vdW) interactions. Such a unique structure endows $MoS_2$ many excellent catalytic,[1−3] photovoltaic,[4,5] and lubricant properties,[6−8] and at the same time provides sufficient interlayer spaces for intercalating foreign molecules and atoms.[9−12]

Nowadays lithium ion batteries (LIBs) are widely used as energy storage media for consumer electronics and are also promising for electric vehicles and electric grid applications, among others. Normally an LIB consists of anode, cathode, and electrolyte. The anode of LIBs is usually made from carbon materials, whereas the cathode is usually built out of metal oxide. Ideally, a good cathode material should have high Li intercalation voltage, whereas a good anode material should have low Li deintercalation voltage, and both cathode and anode materials prefer high Li mobility.[13,14] Because of the unique layered structure, $MoS_2$ highly favors the reversible $Li^+$ intercalation/deintercalation and has long been considered to be an ideal electrode material for advanced LIBs.[15−19]

The recent breakthroughs in fabricating $MoS_2$ nanostructures[20−26] make $MoS_2$ even more attractive for LIB applications because in nanostructures the Li diffusion path could be significantly shortened. For example, Dominko et al.[27] demonstrated that $MoS_2$ nanotubes have highly reversible capacity (~385 mAh/g) and excellent cycle stability. In particular, several groups[28−31] found that restacked $MoS_2$ nanoplates exhibit superior rate capability and cycling stability as anode materials for LIBs. They attributed the better performance of restacked $MoS_2$ layers to the enlarged lattice parameter in the *c* direction and surface area, which facilitate the Li diffusion and intercalation. Following this argument, we can expect that $MoS_2$ monolayer, which can be obtained by further exfoliating $MoS_2$ nanoplates, has even better performance as LIB electrode materials.

Recently, 2-D $MoS_2$ nanosheets with one or few layers have been achieved through different methods,[32−40] and their applications have been explored, such as in nanotransistors.[41−44] More excitingly, shortly after the theoretical predictions,[45,46] Wang et al. realized single-layered $MoS_2$ nanoribbons ($MoS_2NRs$) experimentally.[47]

Not suprisingly, the electrochemistry of $MoS_2$ monolayer-related materials has been attracting a lot of interest ever since their synthesis. Chang et al. synthesized a series of $MoS_2$ sheet/graphene composites that exhibit excellent rate capability and cycling stability as anode materials for LIBs.[48−51] Recently,

**Received:** June 19, 2012
**Accepted:** July 29, 2012

 © XXXX American Chemical Society  dx.doi.org/10.1021/jz300792n | *J. Phys. Chem. Lett.* 2012, 3, 2221−2227

Liang et al. demonstrated experimentally that highly exfoliated graphene-like $MoS_2$ monolayer is a good cathode material of magnesium (Mg) batteries.[52] Yang et al. theoretically predicted that $MoS_2$NRs could also be promising cathodes of rechargeable Mg batteries.[53] This naturally raises an interesting question: could $MoS_2$ monolayer and nanoribbons have the potential to be used as cathode materals of LIBs? To our best knowledge, this issue has not been addressed until now.

In this work, we systematically investigated the adsorption and diffusion of Li atom on $MoS_2$ bulk, bilayer, monolayer, and zigzag $MoS_2$NRs ($ZMoS_2$NRs) by means of density functional theory (DFT) computations and explored the potential of using $MoS_2$ monolayer and $ZMoS_2$NRs as cathode materials of LIBs. $MoS_2$ bulk binds strongly with Li and has a moderate Li diffusion barrier; Reducing dimensionality to bilayer and monolayer simutaneously decreases the Li binding energy and diffusion barrier. More importantly, because of the edge effect, both the binding strength and the mobility of Li (by lowering the diffusion barrier) can be enhanced in zigzag $MoS_2$ nanoribbons. Therefore, $ZMoS_2$NRs are promising as cathode materials of Li-ion batteries with a high power density and fast charge/discharge rates.

*Computational Details*. Our DFT computations were carried out by using an all-electron method within a generalized gradient approximation (GGA) for the exchange-correlation term, as implemented in the DMol$^3$ code.[54,55] The double numerical plus polarization (DNP) basis set and PW91 functional were adopted.[56] Self-consistent field (SCF) computations were performed with a convergence criterion of $10^{-6}$ a.u. on the total energy and electron density. To ensure high-quality numerical results, we chose the real-space global orbital cutoff radius as high as 4.6 Å in all computations. The Brillouin zones of $MoS_2$ bulk, nanosheets, and nanoribbons were sampled with $4 \times 4 \times 4$, $4 \times 4 \times 1$, and $1 \times 1 \times 8$ $k$ points, respectively. The transition states were located by using the synchronous method with conjugated gradient (CG) refinements.[57] This method involves linear synchronous transit (LST) maximization, followed by repeated CG minimizations, and then quadratic synchronous transit (QST) maximizations and repeated CG minimizations until a transition state is located.

It is well known that standard PW91 function is incapable of giving an accurate description of weak interactions. Therefore, for $MoS_2$ bulk and bilayer, we adopted a DFT+D (D stands for dispersion) approach with the Ortmann–Bechstedt–Schmidt (OBS) vdW correction.[58] This approach is a hybrid semi-empirical solution that introduces dispersion correction of the form $C_6R^{-6}$ in the DFT formalism. The computed lattice constant $c$ of $MoS_2$ bulk (12.37 Å) is in good agreement with experimental value (12.32 Å).[59]

We define the Li binding energy, $E_b$(Li), as $E_b$(Li) = $E_{tot}(MoS_2) + E_{tot}(Li) - E_{tot}(MoS_2{-}Li)$, where $E_{tot}(MoS_2{-}Li)$, $E_{tot}(MoS_2)$, and $E_{tot}$(Li) are the total energies of Li-adsorbed $MoS_2$ (bulk, monolayer, bilayer or nanoribbon), Li atom, and $MoS_2$, respectively. According to this definition, a more positive binding energy indicates a more favorable exothermic lithiation reactions between $MoS_2$ and Li.

*Results and Discussion. Adsorption and Diffusion of a Single Li Atom in Bulk $MoS_2$*. First, we examined the adsorption and diffusion of a single Li atom in bulk phase of $MoS_2$. $MoS_2$ layers can be stacked in two patterns: one is rhombohedral type (3R) with three-molecule layers per unit cell and the other is hexagonal type (2H) with two-molecule layers per unit cell (P63/mmc). However, the most stable form of bulk phase of $MoS_2$ is 2H type,[60] and $MoS_2$ plate-like crystals usually grow in the 2H type, which is a stable form up to 1000 °C.[61] Therefore, only the 2H type was considered in our computations. To avoid the interaction between two Li atoms safely, we used a $4 \times 4 \times 2$ supercell for $MoS_2$ bulk, which consists of 32 Mo atoms and 64 S atoms.

Two representative sites for lithiation are available in $MoS_2$ bulk: (1) the tetrahedral site formed by three S atoms from upper triple layer and one S atom from lower triple layer (Figure 1a) and (2) the octahedral site in which Li can bind to three S atoms from each of the triple layers (Figure 1b).

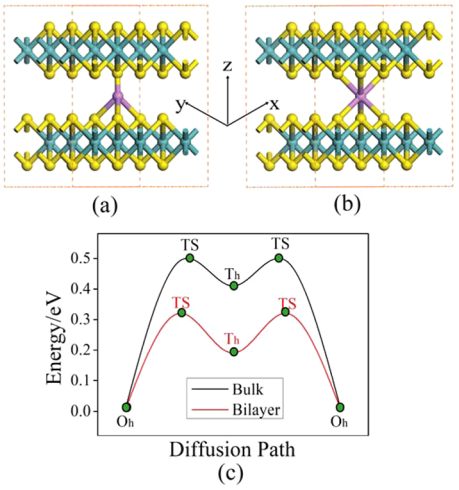


**Figure 1.** Side views of geometries of a Li atom adsorbed at the tetrahedral site (a) and octahedral site (b) of $MoS_2$ bulk. The cyan, yellow, and pink balls denote Mo, S, and Li atoms, respectively. (c) Energy profiles for Li diffusion in $MoS_2$ bulk and bilayer from an octahedral ($O_h$) site to another, passing through a tetrahedral ($T_h$) site.

Our computations show that Li atom prefers to adsorb at the octahedral site (Figure 1b) with a binding energy of 3.08 eV, and the newly formed Li–S bonds are uniformly 2.45 Å. According to the Hirshfeld population analysis, Li possesses only 0.05 lel positive charge, indicating that there is certain covalent component in Li–S bonds. The lithium adsorption at the tetrahedral site is also energetically favorable (with a binding energy of 2.64 eV); in this case, the lengths for upper and lower Li–S bonds are 2.23 and 2.12 Å, respectively, and Li donates 0.06 lel charge to $MoS_2$ bulk.

Then, we studied the Li diffusion in $MoS_2$ bulk between two neighboring octahedral sites, passing through a tetrahedral site by using LST/QST method (Figure 1c). The computed diffusion barrier (0.49 eV) indicates that Li can readily diffuse in bulk $MoS_2$. However, to enhance further the Li mobility, this diffusion barrier still needs to be decreased. It is expected that in exfoliated $MoS_2$ nanosheets Li can diffuse faster than in $MoS_2$ bulk.

*Adsorption and Diffusion of a Single Li Atom in $MoS_2$ Bilayer and Monolayer*. To examine whether the Li mobility can be enhanced in exfoliated $MoS_2$ nanosheets, we investigated the adsorption and diffusion of Li in both $MoS_2$ bilayer and monolayer.

In $MoS_2$ bilayer, the octahedral site is more favorable for lithiation than the tetrahedral site (the binding energies are 2.71 and 2.52 eV, respectively). Note that even the highest Li


dx.doi.org/10.1021/jz300792n | J. Phys. Chem. Lett. 2012, 3, 2221–2227

binding energy in $MoS_2$ bilayer is 0.37 eV lower than that for the most favorable site in $MoS_2$ bulk (3.08 eV). $MoS_2$ bilayer has a little larger interlayer distance than the bulk (6.37 Å vs 6.18 Å). Upon lithiation, the newly formed Li−S bonds at the octahedral site in $MoS_2$ bilayer are also slightly longer than the corresponding ones in $MoS_2$ bulk (2.51 Å vs. 2.45 Å). As expected, the elongated interlayer distances in $MoS_2$ layer lead to the facilitated Li diffusion: the computed Li diffusion barrier between two neighboring octahedral sites in $MoS_2$ bilayer (0.32 eV) is 0.17 eV lower than that of $MoS_2$ bulk (Figure 1b).

When $MoS_2$ bulk is eventually exfoliated into $MoS_2$ monolayer, there are also two representative adsorption sites for Li lithiation, namely, the hollow site (H) above the center of the hexagon (Figure 2a) and the top site (T) directly above one

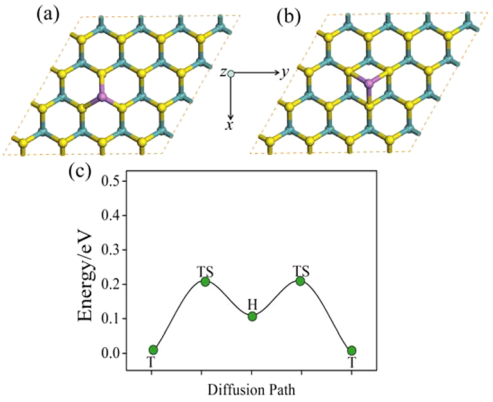


**Figure 2.** Geometries of a Li atom adsorbed at the T site (a) and H site (b) of $MoS_2$ monolayer. (c) Energy profiles for Li diffusion on $MoS_2$ monolayer from a T site to another, passing through an H site.

Mo atom (Figure 2b), which are actually derived from the bulk octahedral and tetrahedral sites, respectively. In both H and T sites, Li atoms are coordinated by three S atoms. We also considered the possibility for the Li atom atop a S atom, but this configuration was excluded because Li moves to the T site spontaneously upon relaxation; similar phenomena were found when adsorbing other metal atoms on $MoS_2$ in previous theoretical studies.[62−65]

The T site is energetically more favorable to bind a lithium atom than the H site (Li binding energies are 2.12 and 2.01 eV for T and H sites, respectively). For lithiation at the T site, the mean Li−S bond length is 2.37 Å, and at this case Li possesses a 0.36 |e| positive charge, which is much more pronounced than that in $MoS_2$ bulk (0.05 |e|). For lithiation at the H site, the mean Li−S bond length is 2.43 Å, and there is about 0.32 |e| charge transfer from Li atom to the $MoS_2$ monolayer.

The diffusion of Li on $MoS_2$ monolayer occurs by migrating from a T site to another, passing through a H site (Figure 2c). The computed energy barrier (0.21 eV) is much lower than that in $MoS_2$ bulk (0.49 eV) and is also lower than that in $MoS_2$ bilayer (0.32 eV). A similar result was also found in $TiS_2$-related materials.[66]

The difference of diffusion barriers among $MoS_2$ bilayer, monolayer, and bulk would have a significant effect on the mobility of Li. By using Arrhenius equation ($D \propto e^{(Ea/kT)}$), we can quantitatively estimate that Li mobility in $MoS_2$ bilayer and monolayer can be increased by a factor of $10^2$ and $10^4$, respectively, compared with that in $MoS_2$ bulk at room temperature.

Although the 2D $MoS_2$ nanosheets have much higher Li mobility, their decreased Li binding energies do not make them ideal candidates for cathode materials. Note that high Li binding energy, or high Li intercalation voltage, is required to ensure the thermodynamic stability in cathodes. Rolling $MoS_2$ nanosheets into nanotubes may increase the Li binding energy due to the curvature effect; however, our computations revealed that the Li bonding energies in thin $MoS_2$ nanotubes are still lower than that in $MoS_2$ bulk. (See the Supporting Information.) Therefore, increasing the Li binding energy without sacrificing the Li mobility is the problem for us to conquer.

*Adsorption and Diffusion of a Single Li Atom in $MoS_2$ Nanoribbons.* Inspired by the theoretical finding by Barone et al.[67] that cutting graphene into graphene nanoribbons (GNRs) can significantly enhance the Li binding energies due to the presence of reactive edges, we expected that the enhanced Li binding could also exist in $MoS_2$NRs. In the following parts, we put our emphasis on the adsorption and diffusion of Li on the $MoS_2$NRs.

Similar to GNRs, two types of $MoS_2$NRs, with zigzag or armchair edges, can be obtained by cutting a $MoS_2$ monolayer. However, previous theoretical studies[45,47] demonstrated that Z$MoS_2$NRs are more stable than the armchair ones, and the experimentally realized $MoS_2$NRs[47] also have zigzag edges. Therefore, in this work, we only considered the Li adsorption and diffusion on the $MoS_2$NRs with zigzag edges. The 8-Z$MoS_2$NR (refer to ref 45 for the definition of the width of $MoS_2$NRs) was chosen as a model for the study. In particular, the Mo edge of 8-Z$MoS_2$NR is half-passivated by S atoms, and the S edge is fully saturated with S atoms, which has been confirmed theoretically to be the energetically most favorable passivation pattern (Figure 3).[47]

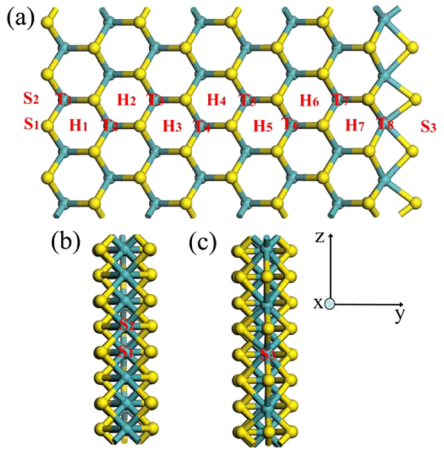


**Figure 3.** (a) Top view of geometry of 8-Z$MoS_2$NR. All examined Li adsorption sites are denoted with red characters. (b,c) Side views of S and Mo edges, respectively.

Because of the unsymmetrical structural property, many more unique sites for lithiation are available along the transverse direction of Z$MoS_2$NRs. In this study, we considered all possible sites throughout the ribbon for Li adsorption on 8-Z$MoS_2$NR, including 8 T sites and 8 H sites on the basal plane and two sites on the side plane ($S_1$,$S_2$). Note that $S_1$ and $S_3$ are two-fold hollow sites, whereas $S_2$ is a four-fold hollow site.

The computed Li binding energies, mean Li−S bond lengths, and the Hirshfeld charges of Li for all the examined sites for 8-


dx.doi.org/10.1021/jz300792n | J. Phys. Chem. Lett. 2012, 3, 2221−2227

**Table 1. Computed Li Binding Energies ($E_b$), Mean Li−S Bond Lengths ($L_{Li-S}$), and Hirshfeld Charges of Li ($Q_{Li}$) for All the Examined Li Adsorption Sites of 8-ZMoS$_2$NR**

| site | $T_1/H_1$ | $T_2/H_2$ | $T_3/H_3$ | $T_4/H_4$ | $T_5/H_5$ | $T_6/H_6$ | $T_7/H_7$ | $S_1/S_2$ | $S_3$ |
|---|---|---|---|---|---|---|---|---|---|
| $E_b$ | 3.59/3.40 | 3.10/2.92 | 2.94/2.79 | 2.85/2.73 | 2.84/2.74 | 2.89/2.80 | 2.96/2.91 | 3.62/3.47 | 3.26 |
| $L_{Li-S}$ | 2.39/2.43 | 2.40/2.43 | 2.40/2.43 | 2.40/2.43 | 2.40/2.43 | 2.39/2.42 | 2.40/2.43 | 2.33/2.71 | 2.32 |
| $Q_{Li}$ | 0.31/0.33 | 0.33/0.35 | 0.33/0.36 | 0.33/0.36 | 0.33/0.36 | 0.33/0.36 | 0.33/0.35 | 0.34/0.36 | 0.40 |

ZMoS$_2$NR are summarized in Table 1. The T8 site does not correspond to a local minimum; upon relaxation, the Li atom at T8 site moves to the edge and binds with two terminal S atoms ($S_3$ site).

Among all the sites of 8-ZMoS$_2$NR considered here, the two-fold hollow $S_1$ site at the edge has the highest Li binding energy (3.62 eV), followed by two other edge sites, namely, the tetrahedral $T_1$ site and four-fold hollow $S_2$ site (3.59 and 3.47 eV, respectively). On the basal plan, the $T_i$ sites are generally energetically more favorable than the corresponding $H_i$ sites, which is similar to the case of MoS$_2$ monolayer. All these examined adsorption sites have a higher Li binding energy than that of MoS$_2$ monolayer, and some sites even have a higher Li binding energy than that of MoS$_2$ bulk, and thus cutting MoS$_2$ monolayer into 1D ZMoS$_2$NRs can effectively enhance the Li binding energy, which is similar to the case of GNRs.[67] Moreover, the sites close to the edges have higher Li binding energies than the inner sites, implying a remarkable edge effect. In particular, the S edge of the ZMoS$_2$NRs is more favorable to bind Li than the Mo edge.

To get a deeper understanding of the mechanism behind the enhanced interaction strength of Li on 8-ZMoS$_2$NR, we computed the density of states (DOS) of 8-ZMoS$_2$NR and compared with that of MoS$_2$ monolayer. Consistent with previous studies,[45,46] 2D MoS$_2$ monolayer is semiconducting with a 1.62 eV band gap (Figure 4a). The conduction band minimum (CBM) and valence band maximum (VBM) are both contributed by the 3d states of Mo atoms throughout the layer (not shown here). In other words, there is no particular reactive site in MoS$_2$ monolayer. In sharp contrast, when MoS$_2$ monolayer is cut into 1D zMoS$_2$NRs, several substantial peaks appear at the zone of Fermi level, which tune 8-ZMoS$_2$NR into metallic (Figure 4b). These metallic states would enhance the interaction between Li and 8-ZMoS$_2$NR and directly lead to the stronger binding among them. Moreover, the metallic states at the zone of Fermi level are mainly contributed by the edge atoms, especially those at the S edge (Figure 4c), which can explain why the edge sites have more pronounced binding energies than the inner sites and the S edge is more favorable for Li binding than the Mo edge. Similar edge states can also be found in zigzag GNRs, which are believed to be responsible for the enhanced Li binding strength at the edge sites.[67] Note that GNRs have been experimentally used as advanced anode materials,[68] whereas ZMoS$_2$NRs are a good candidate for cathode applications.

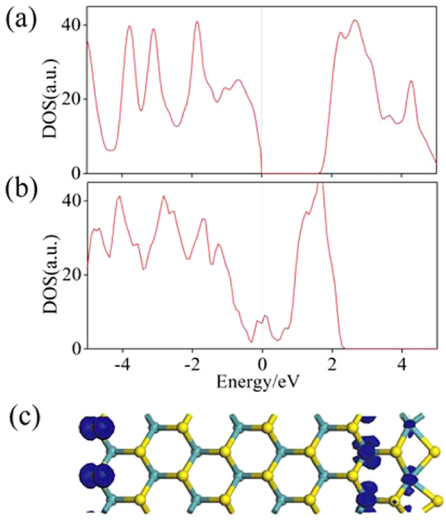


**Figure 4.** Density of states (DOS) of MoS$_2$ monolayer (a) and 8-ZMoS$_2$NR (b). Electronic profile of metallic states at the Fermi level of 8-ZMoS$_2$NR (c).

To examine the edge effect on the Li mobility, we further computed the Li diffusion barrier along different pathways, namely, along the periodic direction (axis direction, Figure 5) and along the transverse direction (Figure 6) of 8-ZMoS$_2$NR.

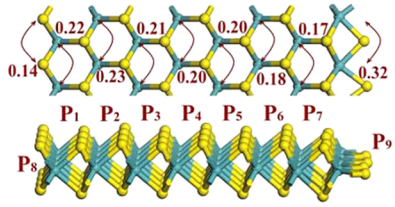


**Figure 5.** Top (upper) and side (bottom) views of Li diffusion paths on 8-ZMoS$_2$NR along the axis direction. The numbers indicate the diffusion barriers in electronvolts. The double-headed arrows denote that Li atoms can diffuse in two directions.

Along the periodic direction of 8-ZMoS$_2$NR, seven diffusion paths ($P_i = T_i \rightarrow H_i \rightarrow T_i$, $i = 1-7$) on the basal plan and two diffusion paths ($P_8 = S_2 \rightarrow S_1 \rightarrow S_2$, $P_9 = S_3 \rightarrow S_3$) on the side plan can be identified (Figure 5). Similar to the case of binding energies, the Li diffusion barriers are also very sensitive to whether the binding sites are close to the edge or not. On the basal plan, the Li diffusion barrier decreases gradually from the S edge to the Mo edge, and some diffusion paths even have a lower energy barrier than that of MoS$_2$ monolayer. The lowest (0.14 eV) and the highest (0.32 eV) diffusion barriers both come from the diffusion paths of side plane. On the side plane of S edge, a Li atom only needs to conquer an energy barrier of 0.14 eV to migrate from a $S_1$ site to another, passing through a $S_2$ site.

However, the pathways along the transverse direction on the basal plane of 8-ZMoS$_2$NR ($P_{10} = T_5 \cdots \rightarrow \cdots T_1$, $P_{11} = T_5 \rightarrow T_6 \rightarrow T_7$, see Figure 6) have lower activation barriers than the axis direction considered above; thus in reality, the Li atoms will prefer the migration along the transverse direction. Regardless where the Li atom is adsorbed on the nanoribbon, it will migrate to the edge by crossing the activation barriers, which decrease gradually toward the edge. If the Li atom is first adsorbed at the site near the S edge, then it will prefer to diffuse toward the S edge, otherwise toward the Mo edge (Figure


dx.doi.org/10.1021/jz300792n | J. Phys. Chem. Lett. 2012, 3, 2221−2227

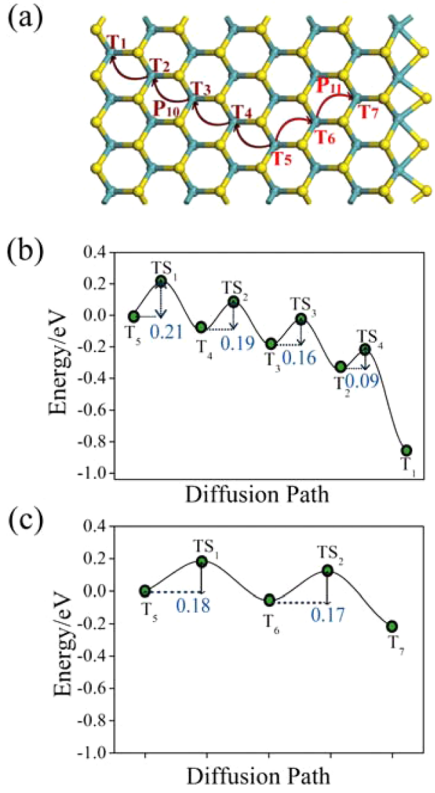


**Figure 6.** (a) Schematic representation of two diffusion paths ($P_{10}$,$P_{11}$) on the basal plane of 8-Z$MoS_2$NR along the transverse direction. (b,c) Energy profiles for $P_{10}$ and $P_{11}$, respectively.

6b,c). This edge-preferred Li diffusion, which was also found in GNRs,[69] may be explained by the unique edge effects. In comparison, in the nanostructures without strong edge effects, such as Si nanowires, Li prefers to diffusion from the surface to the center rather than the opposite direction.[70−72] Overall, the above results imply that once used as LIB cathode materials, Z$MoS_2$NRs can present fast charge/discharge capability.

*Conclusions*. To summarize, we performed DFT computations to disclose the Li adsorption and diffusion in $MoS_2$ bulk, bilayer, monolayer, and Z$MoS_2$NRs. Comprehensive computations demonstrated that the Li mobility can be enhanced by the dimensionality reduction. However, the Li binding energy of $MoS_2$ nanosheets is lower than that of $MoS_2$ bulk, which makes $MoS_2$ nanosheets not ideal candidate for cathode applications. Cutting $MoS_2$ nanosheets into Z$MoS_2$NRs can significantly enhance the Li binding energy and at the same time preserve the high Li mobility. Therefore, Z$MoS_2$NRs, which have been recently realized experimentally, are promising as cathode materials of Li-ion batteries with high power densities and fast charge/discharge rates. Our theoretical studies will hopefully inspire experimental studies on Z$MoS_2$NRs as cathode materials.

## ■ ASSOCIATED CONTENT

### Supporting Information

Variation of the binding energy of Li on the outside surface T site of $(n,n)$ $(6 \leq n \leq 10)$ and $(n,0)$ $(9 \leq n \leq 14)$ $MoS_2$ nanotubes as a function of tube diameter. This material is available free of charge via the Internet at http://pubs.acs.org.

## ■ AUTHOR INFORMATION

### Corresponding Author

*E-mail: zhouzhen@nankai.edu.cn (Z.Z.); zhongfangchen@gmail.com (Z.C.).

### Notes

The authors declare no competing financial interest.

## ■ ACKNOWLEDGMENTS

Support in China by NSFC (21073096), MOE Innovation Team (IRT0927), 111 Project (B12015), and the Fundamental Research Funds for the Central Universities and in the USA by NSF Grant EPS-1010094 and Department of Defense (Grant W911NF-12-1-0083) is gratefully acknowledged. The computations were partially performed on TianHe-1(A) at National Supercomputer Center in Tianjin, China.

## ■ REFERENCES

(1) Paskach, Y. J.; Schrader, G. L.; McCarley, R. E. Synthesis of Methanethiol from Methanol over Reduced Molybdenum Sulfide Catalysts Based on the $Mo_6S_8$ Cluster. *J. Catal.* **2002**, *211*, 285−295.

(2) Chen, J.; Li, S. L.; Xu, Q.; Tanaka, K. Synthesis of Open-Ended $MoS_2$ Nanotubes and the Application As the Catalyst of Methanation. *Chem. Commun.* **2002**, 1722−1723.

(3) Cheng, F. Y.; Chen, J.; Gou, X. L. $MoS_2$-Ni Nanocomposites as Catalysts for Hydrodesulfurization of Thiophene and Thiophene Derivatives. *Adv. Mater.* **2006**, *18*, 2561−2564.

(4) Fortin, E.; Sears, W. M. Photovoltaic Effect and Optical Adsorption in $MoS_2$. *J. Phys. Chem. Solids.* **1982**, *43*, 881−884.

(5) Bernede, J. C.; Pouzet, J.; Gourmelon, E.; Hadouda, H. Recent Studies on Photoconductive Thin Films of Binary Compounds. *Synth. Met.* **1999**, *99*, 45−52.

(6) Chhowalla, M.; Amaratunga, G. A. J. Thin Films of Fullerene-Like $MoS_2$ Nanoparticles with Ultra-Low Friction and Wear. *Nature* **2000**, *407*, 164−167.

(7) Muratore, C.; Voevodin, A. A. Molybdenum Disulfide as a Lubricant and Catalyst in Adaptive Nanocomposite Coatings. *Surf. Coat. Technol.* **2006**, *201*, 4125−4130.

(8) Stefanov, M.; Enyashin, A. N.; Heine, T.; Seifer, G. Nano-lubrication: How Do $MoS_2$-Based Nanostructures Lubricate? *J. Phys. Chem. C* **2008**, *112*, 17764−17767.

(9) For a recent review, see: Benavente, E.; Santa Ana, M. A.; Mendizábal, F.; González, G. Intercalation Chemistry of Molybdenum Disulfide. *Coord. Chem. Rev.* **2002**, *224*, 87−109.

(10) Remškar, M.; Škraba, Z.; Stadelmann, P.; Lévy, F. Structural Stabilization of New Compounds. $MoS_2$ and $WS_2$ Micro- and Nanotubes Alloyed with Gold and Silver. *Adv. Mater.* **2000**, *12*, 814−818.

(11) Chen, J.; Kuriyama, N.; Yuan, H.; Takeshita, H. T.; Sakai, T. Electrochemical Hydrogen Storage in $MoS_2$ Nanotubes. *J. Am. Chem. Soc.* **2001**, *123*, 11813−11814.

(12) Remškar, M.; Mrzel, A.; Viršek, M.; Jesih, A. Inorganic Nanotubes as Nanoreactors: The First $MoS_2$ Nanopods. *Adv. Mater.* **2007**, *19*, 4276−4278.

(13) Meng, Y. S.; Arroyo-de Dompablo, M. E. First Principles Computations Materials Design for Energy Storage Materials in Lithium Ion Batteries. *Energy Environ. Sci.* **2009**, *2*, 589−609.

(14) Whittingham, M. S. Lithium Batteries and Cathode Materials. *Chem. Rev.* **2004**, *104*, 4271−4301.

(15) Py, M. A.; Haering, R. R. Structural Destabilization Induced by Lithium Intercalation in $MoS_2$ and Related Compounds. *Can. J. Phys.* **1983**, *61*, 76−84.

(16) Samaras, I.; Saikh, S. I.; Julien, C.; Balkanski, M. Lithium Insertion in Layered Materials as Battery Cathodes. *Mater. Sci. Eng., B* **1989**, *3*, 209−214.

(17) Julien, C.; Saikh, S. I.; Nazri, G. A. Electrochemical Studies of Disordered $MoS_2$ as Cathode Material in Lithium Batteries. *Mater. Sci. Eng., B* **1992**, *15*, 73−77.

(18) Miki, Y.; Nakazato, D.; Ikuta, H.; Uchida, T.; Wakihara, M. Amorphous $MoS_2$ as the Cathode of Lithium Secondary Batteries. *J. Power. Sources* **1995**, *54*, 508−510.
(19) Santiago, Y.; Cabrera, C. R. Surface Analysis and Electrochemistry of $MoS_2$ Thin Films Prepared by Intercalation-Exfoliation Techniques. *J. Electrochem. Soc.* **1994**, *141*, 629−635.
(20) Remškar, M. Inorganic Nanotubes. *Adv. Mater.* **2004**, *16*, 1497−1504.
(21) Tenne, R. Inorganic Nanotubes and Fullerene-Like Nanoparticles. *Nat. Nanotechnol* **2006**, *1*, 103−111.
(22) Tenne, R.; Remškar, M.; Enyashin, A.; Seifert, G. Inorganic Nanotubes and Fullerene-Like Structures. *Top. Appl. Phys.* **2008**, *111*, 631−671.
(23) Tenne, R. Inorganic Nanotubes and Fullerene-Like Nanoparticles. *J. Mater. Res.* **2006**, *21*, 2726−2743.
(24) Tenne, R.; Margulis, L.; Genut, M.; Hodes, G. Polyhedral and Cylindrical Structures of Tungsten Disulphide. *Nature* **1992**, *360*, 444−446.
(25) Margulis, L.; Salitra, G.; Tenne, R.; Tallanker, M. Nested Fullerene-Like Structures. *Nature* **1993**, *365*, 113.
(26) Li, X. L.; Li, Y. D. $MoS_2$ Nanostructures: Synthesis and Electrochemical $Mg^{2+}$ Intercalation. *J. Phys. Chem. B* **2004**, *108*, 13893.
(27) Dominko, R.; Arcon, D.; Mrzel, A.; Zorko, A.; Cevc, P.; Venturini, P.; Gaberscek, M.; Remškar, M.; Mihailovic, D. Dichalcogenide Nanotube Electrodes for Li-Ion Batteries. *Adv. Mater.* **2002**, *14*, 1531−1534.
(28) Feng, C. Q.; Ma, J.; Li, H.; Zeng, R.; Guo, Z. P.; Liu, H. K. Synthesis of Molybdenum Disulfides ($MoS_2$) for Lithium Ion Battery Applications. *Mater. Res. Bull.* **2009**, *44*, 1811−1815.
(29) Wang, Q.; Li, J. H. Facilitated Lithium Storage in $MoS_2$ Overlayers Supported on Coaxial Carbon Nanotubes. *J. Phys. Chem. C* **2007**, *111*, 1675−1682.
(30) Du, G. D.; Guo, Z. P.; Wang, S. Q.; Zeng, R.; Chen, Z. X.; Liu, H. K. Superior Stability and High Capacity of Restacked Molybdenum Disulfide as Anode Material for Lithium Ion Batteries. *Chem. Commun.* **2010**, *46*, 1106−1108.
(31) Hwang, H.; Kin, H.; Cho, J. $MoS_2$ Nanoplates Consisting of Disordered Graphene-Like Layers for High Rate Lithium Battery Anode Materials. *Nano Lett.* **2011**, *11*, 4826−4830.
(32) Ramakrishna Matte, H. S. S.; Gomathi, A.; Manna., A. K.; Late, D. J.; Datta, R.; Pati, S. W.; Rao, C. N. R. $MoS_2$ and $WS_2$ Analogues of Graphene. *Angew. Chem.* **2010**, *122*, 4153−4156.
(33) Kisielowski, C.; Ramasse, Q.; Hansen, L.; Brorson, M.; Carlsson, A.; Molenbroek, A.; Topsøe, H.; Helveg, S. Imaging $MoS_2$ Nanocatalysts with Single-Atom Sensitivity. *Angew.Chem., Int. Ed.* **2010**, *49*, 2708−2710.
(34) Coleman, J. N.; Lotya, M.; Neil, A. O.; Bergin, S. D.; King, P. J.; Khan, U.; Young, K.; Gaucher, A.; De, S.; Smith, R. J.; et al. Two Dimensional Nanosheets Produced by Liquid Exfoliation of Layered Materials. *Science* **2011**, *331*, 568−571.
(35) Brivio, J.; Alexander, D. T. L.; Kis, A. Ripples and Layers in Ultrathin $MoS_2$ Membranes. *Nano Lett.* **2011**, *11*, 5148−5153.
(36) Liu, K. K.; Zhang, W.; Lee, Y. H.; Lin, Y. C.; Chang, M. T.; Su, C. Y.; Chang, C. S.; Li, H.; Shi, Y. M.; Zhang, H.; Lai, C. S.; Li, L. J. Growth of Large-Area and Highly Crystalline $MoS_2$ Thin Layers on Insulating Substrates. *Nano Lett.* **2012**, *12*, 1538−1544.
(37) Li, H.; Lu, G.; Yin, Z. Y.; He, Q. Y.; Li, H.; Zhang, Q.; Zhang, H. Optical Identification of Single- and Few-Layer $MoS_2$ Sheets. *Small* **2012**, *8*, 682−686.
(38) Shi, Y.; Zhou, W.; Lu, A. Y.; Fang, W.; Lee, Y. H.; Hsu, A. L.; Kim, S. M.; Kim, K. K.; Yang, H. Y.; Li, L. J.; Idrobo, J. C.; Kong, J. van der Waals Epitaxy of $MoS_2$ Layers Using Graphene As Growth Template. *Nano Lett.* **2012**, *12*, 2784−2791.
(39) Castellanos-Gomez, A.; Barkelid, M.; Goossens, A. M.; Calado, V. E.; van der Zant, H. S. J.; Steele, G. A. Laser-Thinning of $MoS_2$: On Demand Generation of a Single-Layer Semiconductor. *Nano Lett.* **2012**, *12*, 3187−3192.
(40) O'Neill, A.; Khan, U.; Coleman, J. N. Preparation of High Concentration Dispersions of Exfoliated $MoS_2$ with Increased Flake Size. *Chem. Mater.* **2012**, *24*, 2414−2421.
(41) Radisavljevic, B.; Radenovic, A.; Brivio, J.; Giacometti, V.; Kia, A. Single-Layer $MoS_2$ Transistors. *Nat. Nanotechnol.* **2011**, *6*, 147−150.
(42) Li, H.; Yin, Z.; He, Q.; Li, H.; Huang, X.; Lu, G.; Fan, D. W. H.; Tok, A. I. Y.; Zhang, Q.; Zhang, H. Layered Nanomaterials: Fabrication of Single- and Multilayer $MoS_2$ Film-Based Field-Effect Transistors for Sensing NO at Room Temperature. *Small* **2012**, *8*, 63−67.
(43) Yin, Z. Y.; Li, H.; Li, H.; Jiang, L.; Shi, Y. M.; Sun, Y. H.; Lu, G.; Zhang, Q.; Chen, X. D.; Zhang, H. Single-Layer $MoS_2$ Phototransistors. *ACS Nano* **2012**, *6*, 74−80.
(44) Li, H.; Yin, Z. Y.; He, Q. Y.; Li, H.; Huang, X.; Lu, G.; Fam, D. W. H.; Tok, A. I. Y.; Zhang, Q.; Zhang, H. Fabrication of Single- and Multilayer $MoS_2$ Film-Based Field Effect Transistors for Sensing NO at Room Temperature. *Small* **2012**, *8*, 63−67.
(45) Li, Y.; Zhou, Z.; Zhang, S.; Chen, Z. $MoS_2$ Nanoribbons: High Stability and Unusual Electronic and Magnetic Properties. *J. Am. Chem. Soc.* **2008**, *130*, 16739−16744.
(46) Botello-Mendez, A. R.; Lopez-Urias, F.; Terrones, M.; Terrones, H. Metallic and Ferromagnetic Edges in Molybdenum Disulfide Nanoribbons. *Nanotechnology* **2009**, *20*, 325703.
(47) Wang, Z.; Li, H.; Liu, Z.; Shi, Z.; Lu, J.; Suenaga, K.; Joung, S.-K.; Okazaki, T.; Gu, Z.; Zhou, J.; Gao, Z.; Li, G.; Sanvito, S.; Wang, E.; Iijima, S. Mixed Low-Dimensional Nanomaterial: 2D Ultranarrow $MoS_2$ Inorganic Nanoribbons Encapsulated in Quasi-1D Carbon Nanotubes. *J. Am. Chem. Soc.* **2010**, *132*, 13840−13847.
(48) Chang, K.; Chen, W. X. *In Situ* Synthesis of $MoS_2$/Graphene Nanosheet Composites with Extraordinarily High Electrochemical Performance for Lithium Ion Batteries. *Chem. Commun.* **2011**, *47*, 4252−4254.
(49) Chang, K.; Chen, W. X. Single-Layer $MoS_2$/Graphene Dispersed in Amorphous Carbon: Towards High Electrochemical Performances in Rechargeable Lithium Ion Batteries. *J. Mater. Chem.* **2011**, *21*, 17175−17184.
(50) Chang, K.; Chen, W. X.; Ma, L.; Li, H.; Li, H.; Huang, F.; Xu, Z. D.; Zhang, Q.; Lee, J. Y. Graphene-like $MoS_2$/Amorphous Carbon Composites with High and Excellent Stability as Anode Materials for Lithium Ion Batteries. *J. Mater. Chem.* **2011**, *21*, 6251−6257.
(51) Chang, K.; Chen, W. X. L-Cysteine-Assisted Synthesis of Layered $MoS_2$/Graphene Composites with Excellent Electrochemical Performances for Lithium Ion Batteries. *ACS Nano* **2011**, *5*, 4720−4728.
(52) Liang, Y.; Feng, R.; Yang, S.; Ma, H.; Liang, J.; Chen, J. Rechargeable Mg Batteries with Graphene-Like $MoS_2$ Cathode and Ultrasmall Mg Nanoparticle Anode. *Adv. Mater.* **2011**, *23*, 640−643.
(53) Yang, S. Q.; Li, D. X.; Zhang, T. R.; Tao, Z. L.; Chen, J. First-Principles Study of Zigzag $MoS_2$ Nanoribbon As a Promising Cathode Material for Rechargeable Mg Batteries. *J. Phys. Chem. C* **2012**, *116*, 1307−1312.
(54) Delley, B. An All-Electron Numerical Method for Solving the Local Density Functional for Polyatomic Molecules. *J. Chem. Phys.* **1990**, *92*, 508−517.
(55) Delley, B. From Molecules to Solids with the $DMol^3$ Approach. *J. Chem. Phys.* **2000**, *113*, 7756−7764.
(56) Perdew, J. P.; Wang, Y. Accurate and Simple Analytic Representations of the Electron-Gas Correlation Energy. *Phys. Rev. B* **1992**, *45*, 13244−13249.
(57) Govind, N.; Petersen, M.; Gitzgerald, G.; King-Smith, D.; Andzelm, J. A Generalized Synchronous Transit Method for Transition State Location. *J. Comput. Mater. Sci.* **2003**, *28*, 250−258.
(58) Ortmann, F.; Bechstedt, F.; Schmidt, W. G. Semiempirical van der Waals Correction to the Density Functional Description of Solids and Molecular Structures. *Phys. Rev. B* **2006**, *73*, 205101.
(59) Pektov, V.; Billinge, S. J. L.; Larson, P.; Mahanti, S. D.; Vogt, T.; Rangan, K. K.; Kanatzidis, M. G. Structure of Nanocrystalline

Materials Using Atomic Pair Distribution Function Analysis: Study of $LiMoS_2$. *Phys. Rev. B* **2002**, *65*, 0921051−0921054.
(60) Seifert, G.; Terrones, H.; Terrones, M.; Jungnickel, G.; Frauenheim, T. Structure and Electronic Properties of $MoS_2$ Nanotubes. *Phys. Rev. Lett.* **2000**, *85*, 146−149.
(61) Wilson, J. A.; Yoffe., A. D. The Transition Metal Dichalcogenides Discussion and Interpretation of the Observed Optical, Electrical and Structural Properties. *Adv. Phys.* **1969**, *18*, 193−335.
(62) Sorescu, D. C.; Sholl, D. S.; Cugini, A. V. Density Functional Theory Studies of Chemisorption and Diffusion Properties of Ni and Ni-Thiophene Complexes on the $MoS_2$ Basal Plane. *J. Phys. Chem. B* **2003**, *107*, 1988−2000.
(63) Sorescu, D. C.; Sholl, D. S.; Cugini, A. V. Density Functional Theory Studies of the Interaction of H, S, Ni-H, and Ni-S Complexes with the $MoS_2$ Basal Plane. *J. Phys. Chem. B* **2004**, *108*, 239−249.
(64) Andersen, A.; Kathmann, S. M.; Lilga, M. A.; Albrecht, K. O.; Hallen, R. T.; Mei, D. H. Adsorption of Potassium on $MoS_2$(100) Surface: A First-Principles Investigation. *J. Phys. Chem. C* **2011**, *115*, 9025−9040.
(65) Andersen, A.; Kathmann, S. M.; Lilga, M. A.; Albrecht, K. O.; Hallen, R. T.; Mei, D. H. First-Principles Characterization of Potassium Intercalation in Hexagonal 2H-$MoS_2$. *J. Phys. Chem. C* **2011**, *116*, 1826−1832.
(66) Tibbetts, K.; Miranda, C. R.; Meng, Y. S.; Ceder, G. An Ab Initio Study of Lithium Diffusion in Titanium Disulfide Nanotubes. *Chem. Mater.* **2007**, *19*, 5302−5308.
(67) Uthaisar, C.; Barone, V.; Peralta, J. E. Lithium Adsorption on Zigzag Graphene Ribbons. *J. Appl. Chem.* **2009**, *106*, 113715.
(68) Bhardwaj, T.; Antic, A.; Pavan, B.; Barone, V.; Fahlman, B. D. Enhanced Electrochemical Lithium Storage by Graphene Nanoribbons. *J. Am. Chem. Soc.* **2010**, *132*, 12556−12558.
(69) Uthaisar, U.; Barone, V. Edge Effects on the Characteristics of Li Diffusion in Graphene. *Nano Lett.* **2010**, *10*, 2838−2842.
(70) Chan, T.-L.; Chelikowsky, J. R. Controlling Diffusion of Lithium in Silicon Nanostructures. *Nano Lett.* **2010**, *10*, 821−825.
(71) Zhang, Q. F.; Zhang, W. X.; Wang, W. H.; Cui, Y.; Wang, E. G. Lithium Insertion in Silicon Nanowires: An Ab Initio Study. *Nano Lett.* **2010**, *10*, 3243−3249.
(72) Zhang, Q. F.; Cui, Y.; Wang, E. G. Anisotropic Lithium Insertion Behavior in Silicon Nanowires: Binding Energy, Diffusion Barrier, and Strain Effect. *J. Phys. Chem. C* **2011**, *115*, 9376−9381.